Isobaric-multiplet mass equation in a macroscopic-microscopic approach

O. Klochko[1,2,*] and N. A. Smirnova[3,†]

[1]*The Haberdashers Askes Boys School, Butterfly Lane, Elstree, Hertfordshire WD6 3AF, United Kingdom*
[2]*Department of Mechanical Engineering, University College London, Torrington Place, London WC1E 7JE, United Kingdom*
[3]*CENBG (CNRS/IN2P3 - Université de Bordeaux), 33175 Gradignan Cedex, France*

We study the *a*, *b*, and *c* coefficients of the isobaric-multiplet mass equation (IMME) using a macroscopic-microscopic approach developed by P. Möller and collaborators [At. Data Nucl. Data Tables **59**, 185 (1995); **109-110**, 1 (2016)]. We show that already the macroscopic part of the finite-range liquid-drop model (FRLDM) describes the general trend of the *a* and *b* coefficients relatively well, while the staggering behavior of *b* coefficients for doublets and quartets can be understood in terms of the difference of average proton and neutron pairing energies. The sets of isobaric masses, predicted by the full macroscopic-microscopic approaches, are used to explore the general trends of IMME coefficients up to $A = 100$. We conclude that while the agreement for *a* coefficients is quite satisfactory, the full approaches have less sensitivity to predict the IMME *b* and *c* coefficients in detail. The best set of theoretical *b* coefficients, as given by the modified macroscopic part of the FRLDM, is used to predict masses of proton-rich nuclei based on the known experimental masses of neutron-rich mirror partners, and subsequently to investigate their one- and two-proton separation energies in proton-rich nuclei up to the $A = 100$ region. The estimated position of the proton drip line is in fair agreement with known experimental data. These masses are important for simulations of the astrophysical *rp* process.

I. INTRODUCTION

The concept of isospin was introduced by Heisenberg in 1939 [1]. Since then, it has represented a very useful paradigm in nuclear and particle physics, providing more beauty and simplification in theoretical modeling and interpretation of hadron or nuclear properties.

According to the isospin formalism, a nucleon is an isospin $t = 1/2$ baryon, with a neutron and a proton being assigned $t_z = 1/2$ and $t_z = -1/2$, respectively. The three Cartesian components of the isospin operator $\hat{\mathbf{t}}$ obey the $su(2)$ commutation relations,

$$[\hat{t}_i, \hat{t}_j] = i\varepsilon_{ijk}\hat{t}_k \qquad (1)$$

and $[\hat{\mathbf{t}}^2, \hat{t}_i] = 0$, where i, j, k run over x, y, z, and $\hat{\mathbf{t}}^2 = \hat{t}_x^2 + \hat{t}_y^2 + \hat{t}_z^2$.

In the absence of electromagnetic interactions and under the assumption of equal proton and neutron masses, a Hamiltonian of a nucleus would commute with the many-body isospin operator, $\hat{\mathbf{T}} = \sum_{n=1}^{A} \hat{\mathbf{t}}(n)$, and its eigenstates would represent degenerate isospin multiplets $|TT_z\rangle$, characterized by two quantum numbers, T and T_z, with $T_z = -T, -T + 1, \ldots, T$ [see Fig. 1(a) for illustration]. The members of the isobaric multiplets are called *isobaric analog states*. For a given nucleus, $T_z = (N - Z)/2$ and the isospin quantum number can take values for different states of $T = |T_z|, |T_z| + 1, \ldots, A/2$.

The presence of the Coulomb interaction between protons and possible small isospin-nonconserving forces of nuclear origin break the isospin symmetry. Assuming a two-body nature of charge-dependent forces and conservation of the isospin of a two-nucleon system, Wigner noticed [2] that those isospin-symmetry breaking operators will be a combination of an isoscalar, an isovector, and an isotensor operators. Estimating the splitting of the isobaric multiplets in lowest order perturbation theory due to the expectation value of such an operator, Wigner showed [2] that isobaric multiplets will be split according to a quadratic equation in T_z, called the *isobaric multiplet mass equation* (IMME),

$$M(\eta, T, T_z) = a(\eta, T) + b(\eta, T)T_z + c(\eta, T)T_z^2. \qquad (2)$$

Here, $M(\eta, T, T_z)$ refers to the atomic mass excess, $\eta = (A, J^\pi, N_{exc}, \ldots)$ denotes all other than T quantum numbers (atomic mass number, spin and parity, number of an excited state, etc.), which are required to label a quantum state of an isobaric multiplet, whereas *a*, *b*, and *c* are coefficients. As an example, the splittings of the lowest $T = 1/2$ and $T = 3/2$ isobaric multiplets in $A = 29$ are shown in Fig. 1(b).

There has always been a lot of interest in the IMME, which proved to work for a great number of quartets and quintets as well, serving thus as a ground for nuclear mass models [3]. The properties of the coefficients – their global trends and a specific staggering phenomenon – have been studied theoretically since 1960s [4–7] up to the present (see, e.g., Refs. [8–15] for the very recent work). A particular attention has been paid to experimental search (e.g., [16] and references therein) and theoretical interpretation of cubic or quartic terms
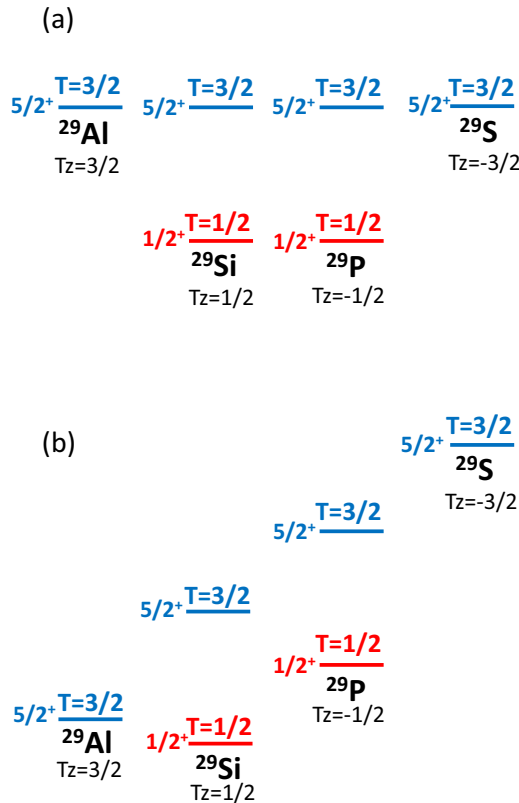
*zcemokl@ucl.ac.uk
†smirnova@cenbg.in2p3.fr

(a)

(b)

FIG. 1. The lowest $T = 1/2$ and $T = 3/2$ isobaric multiplets in $A = 29$: (a) schematic illustration of degenerate multiplets in the absence of charge-dependent interactions; (b) realistic situation obtained using experimental masses excesses of the corresponding nuclei. See text for details.

in the IMME due to isospin mixing or to manifestations of the charge-dependent many-body forces [17–23].

The advent of modern radioactive ion beam facilities, progress in mass measurements and particle detection techniques allowed to access multiplets with more and more short-lived members. The most recent compilations [10,11] of IMME coefficients contain an impressive amount of highly precise data which provides general trends of the IMME coefficients and sometimes staggering effects as a function of A, highlighting specific properties of the nucleon-nucleon interaction and giving certain hints on existing shell effects.

Recent achievements in microscopic many-body theory allow us to calculate IMME parameters using both phenomenological and microscopic effective nucleon-nucleon forces [8,9,13,14,22–27]. In empirical approaches, experimental databases are often used to establish the strength in isovector and isotensor channels of an effective nuclear force. However, to provide a uniform description of the whole region of data from $A = 5$ to $A \approx 100$ nuclei is still challenging.

A particular high interest to masses of proton-rich nuclei up to $A \approx 100$ is also due to their significance for simulations of the astrophysical rp process which powers type-I x-ray bursts [28]. These are periodic events which occur in binary systems consisting of a rapidly rotating neutron star, accreting hydrogen- and helium-rich material from its companion, typ-

ically a main-sequence star. At high temperature and pressure conditions, the burst is ignited, powered by the explosive burning of hydrogen and helium [29]. The radiative proton capture reactions are the most important reaction sequence, which in competition with the β^+ decay is responsible for synthesis of proton-rich nuclides up to the $A = 100$ region. Nuclear physics input on masses, one- and two-proton separation energies, and β-delayed processes are thus of great importance for x-ray burst models for reliable calculations of light curves and predictions of final abundances (see, e.g., Ref. [30] for the current status of state-of-the-art modelizations). This leads to enormous experimental and theoretical efforts to provide astrophysicists with unknown masses of proton-rich nuclei [31]. Because of the complexity of the nuclear many-body problem and extreme conditions, various approaches achieve a consensus on some proton drip-line nuclei, while disagreeing on others. Thus, there is still need for more understanding and more accurate theoretical predictions.

In this work, we propose to construct theoretical a, b, and c coefficients and study their properties using a global macroscopic-microscopic approach developed during a few decades by P. Möller and collaborators [32,33]. This framework, designed for global nuclear mass calculations, consists of two parts: a macroscopic part and a microscopic one. Two different models have been used throughout the years to represent a macroscopic contribution, giving the names to the corresponding approaches: (i) the finite-range liquid-drop model (within the FRLDM), and (ii) the finite-range droplet model (within the FRDM). The former is a far more refined version of the uniformly charged liquid drop model, while the latter includes in addition a few high-order terms in A. In both cases, a similar microscopic term has been used, consisting of a shell-plus-pairing correction. The parameters of the models have been thoroughly adjusted to a large variety of known data on nuclear masses. The details of the approach and parametrization strategy can be found in the original work [32,33].

Although phenomenological, the macroscopic-microscopic models have robust grounds and are optimized to describe a few thousands of nuclear masses (around 2150) with very small root-mean-square (rms) error of around 0.56 MeV (0.66 MeV) for FRDM (FRLDM) [33]. The models have been applied mainly to predict masses of (super)heavy elements and fission barriers. In this work, we apply this approach rather to nuclei along the $N = Z$ line and study the general trends and fine structure of the deduced IMME coefficients as a function of the mass number. Some preliminary expressions for b and c coefficients obtained from the macroscopic part of the FRLDM have already been deduced in Refs. [8,26] and applied for either sd or pf shell nuclei. In the present study, we go beyond and we obtain all IMME coefficients from the macroscopic part of FRLDM and from the full macroscopic-microscopic approaches, and we apply them to the whole range of experimental data (excluding only very light nuclei). Starting with a well-known uniformly charged liquid-drop model in Sec. III, we introduce the macroscopic part of the FRLDM from Ref. [32,33] as a more involved and improved way of global description of the IMME coefficients (Sec. IV). We discuss general trends

provided by the model, as well as showing that the staggering effect of b coefficients can be described by different proton and neutron pairing energy parameters. In Sec. V, we explore the predictions given by the full FRLDM and FRDM [32,33]. Finally, in Sec. VI, we use the macroscopic part of the FRLDM, which provides the "best" set of b coefficients, to calculate masses of proton-rich nuclei in the vicinity of the proton drip line from Mn isotopes up to Te isotopes. We discuss the estimated one- and two-proton separation energies in the context of the available experimental data. The last section summarizes the conclusions and outlines the perspectives of this study.

II. EXPERIMENTAL DETERMINATION OF IMME COEFFICIENTS

Starting from Eq. (2), one can express a, b, and c coefficients for a given isobaric multiplet (η, T) in terms of mass excesses of its members. Denoting $M(\eta, T, T_z) \equiv M_{T_z}$, we get for doublets $(J^\pi, T = 1/2)$ that

$$a = (M_{1/2} + M_{-1/2})/2,$$
$$b = M_{1/2} - M_{-1/2}, \tag{3}$$

while a, b, and c coefficients for triplets $(T = 1)$ can be expressed as

$$a = M_0,$$
$$b = (M_1 - M_{-1})/2 \tag{4}$$
$$c = (M_1 + M_{-1})/2 - M_0.$$

It is obvious from these expressions that ground state mass excesses only can serve to obtain a and b coefficients for ground state doublets and b coefficients for the lowest triplets. Generally, M_0 involves an excited state, which is situated at a particularly high excitation energy in an $N = Z$ even-even nucleus. This prohibits derivation of a and c coefficients for triplets from masses only for detailed comparison with the experimental data.

For quartets $(T = 3/2)$, quintets $(T = 2)$, or other high T multiplets, where masses of more than three members are involved, one determines a, b, and c coefficients by a least-squares fit. For example, for quartets, the mass excesses of the isobaric analog states are related by the IMME coefficients via the following system:

$$M_{3/2} = a + \tfrac{3}{2}b + \tfrac{9}{4}c, \tag{5}$$
$$M_{1/2} = a + \tfrac{1}{2}b + \tfrac{1}{4}c, \tag{6}$$
$$M_{-1/2} = a - \tfrac{1}{2}b + \tfrac{1}{4}c, \tag{7}$$
$$M_{-3/2} = a - \tfrac{3}{2}b + \tfrac{9}{4}c. \tag{8}$$

The members with $T_z = \pm 1/2$ require knowledge of the excitation energy of those states.

In the present study, we approximate b coefficients for $T > 1$ multiplets by their relation to the Coulomb displacement energies between members with $T_z = T$ and $T_z = -T$ [9,34]:

$$b = (M_T - M_{-T})/2T. \tag{9}$$

This turns out to be sufficient for a discussion of the general trends and even of staggering phenomena.

III. IMME COEFFICIENTS FROM A UNIFORMLY CHARGED LIQUID DROP

We start with estimates of the contributions to a, b, and c coefficients from the uniformly charged sphere model [35]. The total Coulomb energy of a uniformly charged spherical nucleus of radius $R = r_0 A^{1/3}$ reads

$$E_{coul} = \frac{3e^2}{5R} Z(Z - 1)$$
$$= \frac{3e^2}{5r_0 A^{\frac{1}{3}}} \left[\frac{A}{4}(A - 2) + (1 - A)T_z + T_z^2 \right], \tag{10}$$

giving rise to the following contributions to the IMME a, b, and c coefficients [20,34]:

$$a = \frac{3e^2}{20r_0} \frac{A(A - 2)}{A^{1/3}}, \tag{11}$$
$$b = -\frac{3e^2}{5r_0} \frac{(A - 1)}{A^{1/3}} + \Delta_{nH}, \tag{12}$$
$$c = \frac{3e^2}{5r_0} \frac{1}{A^{1/3}}, \tag{13}$$

where $e^2 = 1.44$ MeV fm and we use here the value of $r_0 = 1.27$ fm. The quantity $\Delta_{nH} = 782.346$ keV is the difference between the neutron (M_n) and hydrogen (M_H) mass excesses. The smooth trends, given by these equations for b and c coefficients, are shown in Figs. 2(b) and 2(c), respectively (labeled as LDM: liquid-drop model) in comparison with the experimental data on b coefficients for doublets with $A = 17$–71 and c coefficients for triplets with $A = 18$–58. We observe that although the general trends are reproduced, there is a visible mismatch between experimental data and predictions, and there are no characteristic staggering patterns (weakly seen for b coefficients of doublets and a pronounced 'sawtooth effect' of c coefficients for triplets). For large A values, one often uses an approximate form of b coefficients, namely

$$b = -\frac{3e^2}{5r_0} A^{2/3} + \Delta_{nH}, \tag{14}$$

showing that the leading-order term in b coefficients is proportional to $A^{2/3}$.

We do not discuss the trend of the a coefficients, since it requires all other members of the liquid-drop model (known as the Weizsäcker formula) and therefore a careful fitting of its parameters [36].

We also remark that it was noticed long ago that the Coulomb interaction alone, even accurately treated, cannot describe observed Coulomb displacement energies of isobaric multiplets [37]. This conclusion gave rise to a special interest in nuclear models capable of providing contributions other than Coulomb isovector or isotensor contributions to the nuclear binding energy (e.g., see Ref. [38] and references therein for the earlier work on this subject). It is exactly the purpose of this study to address these issues within the macroscopic-microscopic approach of Refs. [32,33].
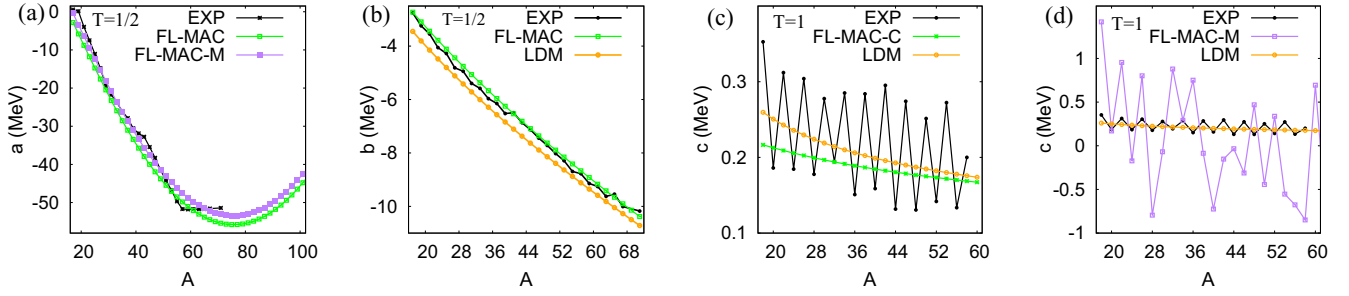
FIG. 2. Theoretical IMME a and b coefficients for doublets [panels (a) and (b), respectively] and c coefficients for triplets [panels (c) and (d)] obtained from the macroscopic part of the FRDLM (FL-MAC) in comparison with experimental data (EXP) and liquid-drop model predictions (LDM). The calculations labeled as FL-MAC-M in panels (a) and (d) refer to the modified macroscopic part of the FRLDM, while calculations labeled as FL-MAC-C on panel (c) designate a Coulomb approximation for c coefficients. Results from the mass models in the last panel have been supplemented by the experimental excitation energy in $T_z = 0$ members. See text for further details.

IV. IMME COEFFICIENTS FROM THE MACROSCOPIC PART OF THE FRLDM

A. General trend

The macroscopic part of the FRLDM proposes a more involved expression for the Coulomb contribution to the atomic mass excess as compared to the liquid-drop model. We adopt the following formulation proposed by Möller *et al.* in Refs. [32,33]:

$$M(Z, A) = M_H Z + M_n(A - Z) \tag{15}$$
$$- a_v(1 - k_v I^2)A \tag{16}$$
$$+ a_s(1 - k_s I^2)B_1 A^{2/3} + a_0 A^0 B_W \tag{17}$$
$$+ c_1 Z^2 B_3/A - c_4 Z^{4/3} B_s/A^{1/3} \tag{18}$$
$$+ f(k_f r_p)Z^2/A - c_a(N - Z) \tag{19}$$
$$+ E_W + E_{\text{pair}} - a_{el}Z^{2.39}, \tag{20}$$

where the first two terms are mass excesses of Z hydrogen atoms and $A - Z = N$ neutrons, followed by the volume term in line (16), then by the surface term and the so-called A^0 energy, a constant, that can be seen in line (17). The parameter B_1 defines the generalized surface energy in the model, and for a spherical nucleus it can be evaluated as

$$B_1 = 1 - \frac{3}{x_0^2} + (1 + x_0)\left(2 + \frac{3}{x_0} + \frac{3}{x_0^3}\right)\exp{(-2x_0)}, \tag{21}$$

with $x_0 = \beta A^{1/3}$, where $r_0 = 1.16$ fm and $\beta = r_0/a \approx 1.706$. We adopt here $B_W = 1$ [32].

Line (18) contains the direct and exchange Coulomb term with $c_1 = 3e^2/(5r_0)$ and $c_4 = 5/4(3/(2\pi))^{2/3}c_1$. The parameter B_3, defining the relative Coulomb energy for an arbitrary shape nucleus, has in leading order (for a spherical nucleus) the following expression:

$$B_3 = 1 - \frac{5}{y_0^2} + \frac{75}{8y_0^3} - \frac{105}{8y_0^5} \tag{22}$$

with $y_0 = \alpha A^{1/3}$, and $\alpha = r_0/a_{\text{den}} \approx 1.657$. We suppose here that the relative surface energy parameter is $B_s = 1$ (a spherical nucleus).

The proton form-factor correction to the Coulomb energy, $f(k_f r_p)$, is parametrized as

$$f(k_F r_p) = -\frac{r_p^2 e^2}{8r_0^3}\left[\frac{145}{48} - \frac{327}{2880}(k_F r_p)^2 + \frac{1527}{1209600}(k_F r_p)^4\right], \tag{23}$$

with the proton radius $r_p = 0.8$ fm, and k_F being the Fermi wave number:

$$k_F = \left(\frac{9\pi Z}{4A}\right)^{1/3}\frac{1}{r_0}. \tag{24}$$

The proton form-factor depends on A, and T_z and varies between about -0.212 and -0.215 for the nuclei of interest, with the average value being -0.2138 MeV for $T_z = 0$ nuclei. We have checked that the resulting rms errors for the IMME coefficients are not very sensitive to this parameter, so we kept the average value for our estimation. The charge-asymmetry term [the second term in line (19)], with the strength c_a, is of pure isovector character and, hence, it will contribute to the b coefficient only [see below Eq. (29)].

The first two terms in line (20) are the Wigner contribution, E_W,

$$E_W = W|I| + \begin{cases} 1/A & \text{if } Z = N \text{ odd}, \\ 0 & \text{otherwise}, \end{cases} \tag{25}$$

and the average pairing term, parametrized as

$$E_{\text{pair}} = \begin{cases} \overline{\Delta}_n + \overline{\Delta}_p - \delta_{pn} & \text{if } Z \text{ odd, } N \text{ odd}, \\ \overline{\Delta}_p & \text{if } Z \text{ odd, } N \text{ even}, \\ \overline{\Delta}_n & \text{if } Z \text{ even, } N \text{ odd}, \\ 0, & \text{if } Z \text{ even, } N \text{ even}. \end{cases} \tag{26}$$

The average neutron and proton pairing gaps and the average neutron-proton interaction energy have been parametrized as

$$\overline{\Delta}_n = \frac{r_n B_s}{N^{1/3}},$$
$$\overline{\Delta}_p = \frac{r_p B_s}{Z^{1/3}}, \tag{27}$$
$$\delta_{np} = \frac{h}{B_s A^{2/3}},$$

with $r_n = r_p = r_{\text{mac}} = 4.80$ MeV being a macroscopic pairing gap parameter. In the original work, this parameter is kept

the same for protons and neutrons. In the present study, we adopted two sets of numerical values of various constants and parameters from both Refs. [32,33]. More details on the model can be found in those references as well. Regarding the macroscopic part of the FRLDM, we find always a somewhat better description when using the parametrization from 1995 [32], so we keep this particular set of parameters in the present section.

The last term in line (20) is the energy of the bound electrons with $a_{el} = 1.433 \times 10^{-5}$ MeV. Due to the smallness of this quantity we neglect this term in the present study.

It is obvious that terms (15)–(19) can be expressed in terms of T_z and A, and thus they can be cast into the form of the IMME. Not considering for the moment the Wigner term and the pairing contribution and keeping up to quadratic terms in $1/A$, one can get the following (approximate) expressions for the IMME a, b, and c coefficients:

$$a = \left(\frac{M_H + M_n}{2} - a_V - \frac{5c_1}{4\alpha^2} - \frac{c_4}{2^{4/3}} + \frac{f(k_f r_p)}{4} \right) A$$
$$+ \frac{1}{4}c_1 A^{5/3} + \left(a_S + \frac{75}{32\alpha^3} \right) A^{2/3}$$
$$- \frac{3a_S}{\beta^2} + a_0 A^0 B_W - \frac{105}{32\alpha^5}, \qquad (28)$$

$$b = \Delta_{nH} - c_1 A^{2/3} - \frac{75c_1}{8\alpha^3} A^{-1/3} - \frac{105c_1}{8\alpha^5} A^{-1}$$
$$- \frac{5c_1}{\alpha^2} - \frac{4c_4}{3(2)^{1/3}} + f(k_f r_p) + 2c_a, \qquad (29)$$

$$c = 4a_V k_V + (c_1 - 4a_S k_S) A^{-1/3}$$
$$- \left(\frac{5c_1}{\alpha^2} + \frac{4c_4}{9(2)^{1/3}} - \frac{12a_S k_S}{\beta^2} - f(k_f r_p) \right) A^{-1}$$
$$+ \frac{75c_1}{8\alpha^3} A^{-4/3} - \frac{105c_1}{8\alpha^5} A^{-2}. \qquad (30)$$

For doublets ($T = 1/2$), it is straightforward to include contributions of the Wigner term and of the pairing term to the a coefficient, which provides the following addition to the a coefficient above:

$$\Delta a_{W+pair} = \frac{W}{A} - r_{mac} B_S \left(\frac{2}{A} \right)^{1/3}, \qquad (31)$$

while no contribution is expected to the doublets' b coefficients if $r_n = r_p$. The resulting numerical expressions are

$$a = 0.1862 A^{5/3} - 8.939 A + 21.586 A^{2/3}$$
$$- 19.420 + 6.048 A^{-1/3} + 30 A^{-1} \text{ [MeV]}, \qquad (32)$$

$$b = -0.7448 A^{2/3} + 2.748 - 1.534 A^{-1/3}$$
$$+ 0.7823 A^{-1} \text{ [MeV]}. \qquad (33)$$

These relations represent a very good approximation to the theoretical a and b coefficients for doublets obtained from the full macroscopic part of FRLDM and are shown in Figs. 2(a) and 2(b) (labeled as FL-MAC) in comparison with the available experimental data. First, we observe that the general trends of a and b coefficients are well reproduced. For a coefficients, it is interesting to note that FRLDM predicts that

the Coulomb term takes over beyond $A \approx 75$, where the a coefficient curve reaches its minimum, and starts to grow for larger values of A. To assess the quality of the results, we use here the rms error, defined as

$$\text{rmse}(x) = \sqrt{\frac{1}{n} \sum_{i=1}^{n} [x_{\text{th}}(i) - x_{exp}(i)]^2}, \qquad (34)$$

where x stands for a, b, or other quantity, $x_{\text{th}}(i)$ are theoretical values, $x_{exp}(i)$ are experimental values, and i runs over the available data points ($i = 1, \ldots, n$). The resulting rms errors of the macroscopic part of the FRLDM for a and b coefficients can be found in Table I (see the entry FL-MAC).

The original parametrization results in relatively large rms errors for the IMME coefficients, as seen from Table I. This is due to the fact that the parameters have been fixed together with the microscopic part (shell correction) of the model. The rms deviations can be greatly improved, if we adjust some selected parameters. To this end, we choose three parameters, namely, a_0, c_a, and r_{mac}, which contribute to the isoscalar, isovector and isotensor channels, and we show that by slightly changing their values we can improve the description of the a, b, and c coefficients, respectively. The corresponding modified version is named FL-MAC-M, where "M" stands for "modified." For example, increasing a_0 from 2.165 to 4.7 MeV, we can reduce the rms error for the a coefficients from 3 to about 1.9 MeV. The modifications of c_a and r_{mac}, which influence b and c coefficients, respectively, will be described below. (To be precise, the parameter r_{mac} also slightly impacts the isoscalar channel: our modification reduces the rms error on the a coefficient by additional 30 keV). The results for the a coefficients obtained from FL-MAC-M are shown in Fig. 2(a).

The macroscopic part of the FRLDM predicts rather well both the trend and the magnitude of b coefficients, leading to a much better agreement with the data than the liquid-drop model. However, it can be noticed that the b coefficients from the FRLDM have a kind of offset with respect to the data. To address this issue, we study various contributions to the b coefficients as easily seen from Eq. (29): The Coulomb direct and exchange terms, the proton form-factor contribution, and the asymmetry term. The general trend is assured by the term ($\sim A^{2/3}$), dominating the Coulomb contribution. The other terms provide (in our approximation) only small constant shifts of b coefficients. Among them, we notice that the proton-neutron asymmetry term contributes only to the b coefficient. We have varied this term and found that a global improvement in the rms error for b coefficients can be achieved by slightly changing its value from $c_a = 0.10289$ MeV to $c_a = 0.186$ MeV: The rms error for a total number of data points reduces from 189 to 91 keV (see the entry FL-MAC-M in Table I). Figure 3 shows this improvement and illustrates the affect of various terms on the b coefficient value, with the new value of c_a taken into account. From now on, we therefore keep this optimized value of c_a in our modified version of the macroscopic part of the FRLDM.

For c coefficients, the implication of terms (15)–(19) is not well defined. As we mentioned in Sec. II, the FRLDM is designed to describe nuclear masses, while to get the c

TABLE I. The rms errors of the IMME a, b, and c coefficients calculated within the macroscopic part of the FRLDM (denoted as FL-MAC), as well as from the full versions of the FRDM and FRLDM as given in Ref. [32] (1995) and [33] (2016). Calculations labeled as FL-MAC-M refer to updated values of a_0, c_a, and r_{mac} with respect to the original model, while FL-MAC-NP exploits in addition the different neutron and proton pairing gap parameters as explained in Sec. IV B. See text for details.

| Model | $T = 1/2$ ($A = 17$–67) | | $T = 1$ ($A = 18$–58) | | $T = 3/2$ ($A = 19$–39) | Total |
	rmse a (keV)	rmse b (keV)	rmse b (keV)	rmse c (keV)	rmse b (keV)	rmse b (keV)
FL-MAC	3009	189	191	841	186	189
FL-MAC-M	1857	113	72	632	75	91
FL-MAC-NP	1857	95	71	632	70	81
FRLDM (1995)	1210	454	416	984	442	438
FRLDM (2016)	1109	434	469	484	529	467
FRDM (1995)	1145	321	250	823	231	278
FRDM (2016)	1062	246	234	1038	227	238

coefficient we have to know the excitation energies of $|T_z| < T$ isobaric-multiplet members (e.g., of the $T_z = 0$ member in triplets). Following Ref. [8], we can restrict ourselves by assuming that only Coulomb terms (both direct and exchange ones) contribute to the c coefficient. This means that we suppose $k_V = k_S = 0$ in Eq. (30), which results in the following numerical expression:

$$c = 0.7448A^{-1/3} - 1.771A^{-1} + 1.535A^{-4/3} - 0.7823A^{-2} \text{ [MeV]}. \quad (35)$$

The corresponding overall trend of c coefficients is shown in Fig. 2(c) (a smooth curve named FL-MAC-C) in comparison with the experimental data on c coefficients for triplets and the liquid-drop model (LDM) predictions.

Alternatively, we can use all isotensor terms of the macroscopic part of the FRLDM, as well as the contribution from the Wigner and pairing terms. Bearing in mind that the model approximates nuclear masses, we take into account the experimentally observed excitation energies of the IAS in $T_z = 0$

FIG. 3. Theoretical IMME b coefficients for doublets: the total value (from FL-MAC-M) and the contribution of different terms from Eq. (29) in comparison with experimental data. The asymmetry parameter is set to $c_a = 0.186$ MeV. See text for further details.

nuclei in order to reconstruct isobaric triplets. By doing this, indeed we get an overall description including a staggering effect. The original parametrization results in the rms error for the c coefficients of triplets of around 841 keV. Again, we checked that increasing a value of the average pairing gap parameter r_{mac} from 4.80 to 5.51 MeV, we can reduce the rms deviation to 632 keV. This value is still too big as compared to the absolute value of the c coefficients (between about 200 and 350 keV), as is easily seen from the resulting curve for the c coefficients shown in Fig. 2(d) (labeled as FL-MAC-M). Although the rms error is reduced, we observe, however, that theoretical c coefficients exhibit staggering of a very large amplitude as compared to experiment. Only up to $A = 28$, this staggering is in phase with the data. For heavier nuclei, oscillations become irregular. This means that the isotensor part of the model is not well constrained by the fit and, therefore, not suitable for understanding the c coefficients. In Sec. V, we will see that the addition of the microscopic part does not remedy the situation.

While it looks difficult to refine the description of the IMME c coefficients in detail, we would be interested in getting a staggering pattern of the b coefficients. This is, however, not provided by the formal analytical expressions of the original macroscopic part of the FRLDM. We address this question in the next section, carefully considering the pairing energy parametrization.

B. Staggering pattern of b coefficients and average proton and neutron pairing gaps

The r_{mac} parameter of the macroscopic part of the FRLDM is an average between proton and neutron pairing energies. As is explained in the original work [32,33], its magnitude is not important for the full model, since it is the microscopic part which is added and optimized to ensure a good agreement with experiment. However, a precise magnitude of the average pairing in the macroscopic part can help us to understand the staggering phenomenon. In the context of different models, this effect has also been discussed in Refs. [4,8,9].

From the study of proton and neutron pairing gaps, we know that those proton and neutron energies may be different. Following the work of Möller and Nix [39], to determine the
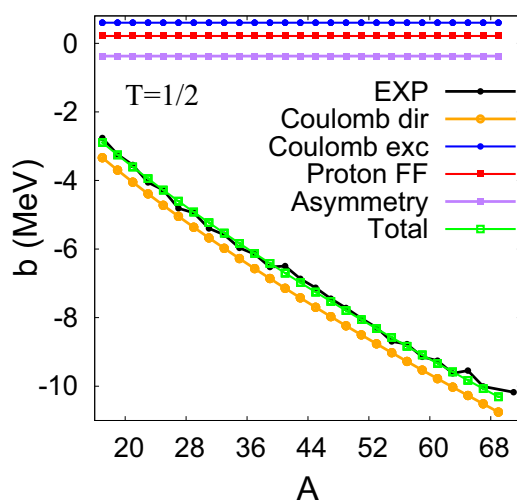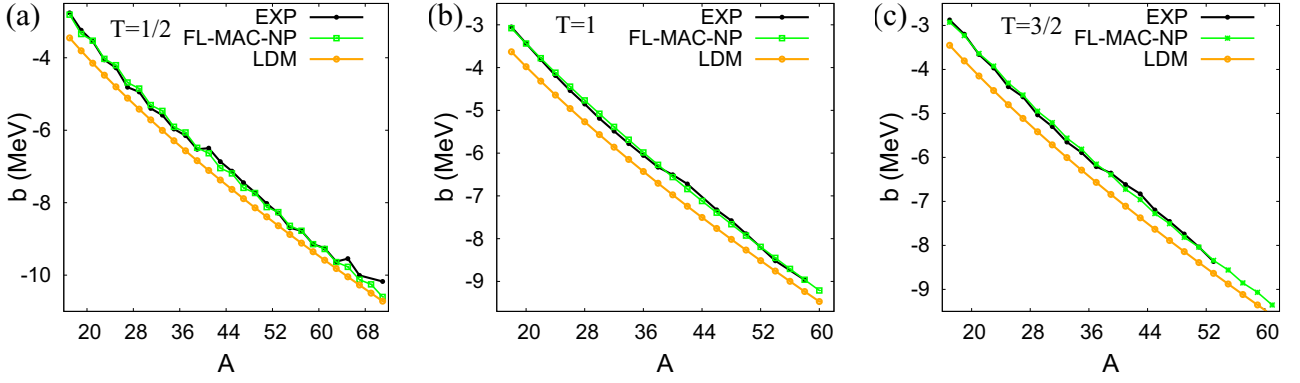
FIG. 4. Theoretical IMME b coefficients for doublets (a), triplets (b), and quartets (c) obtained from the macroscopic part of the FRDLM with different proton and neutron r_n and r_p parameters (FL-MAC-NP) in comparison with experiment.

r_n and r_p parameters separately, we performed a least-squares fit of $\overline{\Delta}_n$ and $\overline{\Delta}_n$ from Eqs. (27) to the experimental neutron and proton pairing gaps, respectively, of nuclei along the $N = Z$ line from $A = 12$ to $A = 74$, which are of interest in our work. The established values are $r_n = 6.83$ MeV and $r_p = 6.65$ MeV, resulting in a difference of $r_n - r_p = 0.18$ MeV. It is this difference between r_n and r_p that leads to the staggering of the b coefficients, as we will show below. The obtained rms errors are summarized in the third line of Table I, referred to as FL-MAC-NP (the parameter $c_a = 0.186$ MeV, as was proposed in the previous section). We see that there is a further improvement in the rms error for the b coefficients compared to FL-MAC-M: it reduces in total from 91 to 81 keV. The corresponding b coefficients for $T = 1/2, 1, 3/2$ multiplets are shown in comparison with experimental data in Fig. 4. Indeed, we notice staggering of the b coefficients for doublets and triplets which is in accord with the experimental data. To better see this effect, we plot in Fig. 5 the quantity $\Delta b = b(A) - b(A - 2)$ for various T multiplets in comparison with the available experimental data. The results on staggering can be understood analytically. The contribution of the pairing term to b coefficients of $A = 4n + 1$ and $A = 4n + 3$ doublets are

$$b_{pair}^{T=1/2} = \begin{cases} (r_n - r_p)\dfrac{2^{1/3}B_s}{(A+1)^{1/3}}, & A = 4n+1, \\[3mm] (r_p - r_n)\dfrac{2^{1/3}B_s}{(A-1)^{1/3}}, & A = 4n+3, \end{cases} \quad (36)$$

which results in a staggering amplitude $\Delta b = b(A) - b(A - 2)$ of

$$\Delta b^{T=1/2} \approx 2(r_n - r_p)\frac{2^{1/3}B_s}{A^{1/3}}, \quad (37)$$

if we assume $A = 4n + 1$. At the same time, for quartets we get the following contributions to the b coefficients:

$$b_{pair}^{T=3/2} = \begin{cases} (r_p - r_n)\dfrac{2^{1/3}B_s}{3(A+3)^{1/3}}, & A = 4n+1, \\[3mm] (r_n - r_p)\dfrac{2^{1/3}B_s}{3(A-3)^{1/3}}, & A = 4n+3, \end{cases} \quad (38)$$

which results in a staggering amplitude of

$$\Delta b^{T=3/2} \approx -2(r_n - r_p)\frac{2^{1/3}B_s}{3A^{1/3}}, \quad (39)$$

if we assume $A = 4n + 1$. This is about of $1/3$ of the amplitude of staggering for doublets in absolute value and is out of phase. The resulting trends of Δb can be seen in Fig. 5 for $T = 1/2$ on the first panel and for $T = 3/2$ multiplets on the third panel in comparison with available experimental data. For reference, we also plot Δb for half-integer values of $T = 1/2, 3/2$, and $5/2$ that comes from the modified macroscopic part of the FRLDM with $r_n = r_p$ (FL-MAC-M): it does not show any staggering.
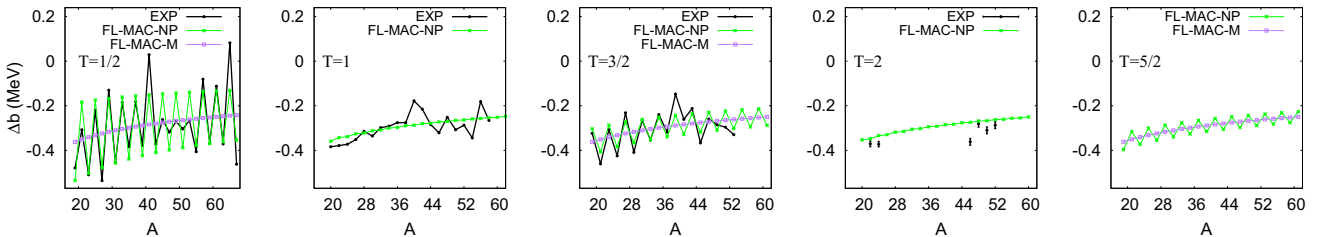

FIG. 5. Differences of IMME b coefficients, $\Delta b = b(A) - b(A - 2)$, for $T = 1/2, 1, 3/2, 2, 5/2$ multiplets as obtained from the modified macroscopic part of the FRDLM with either identical proton and neutron pairing gap parameters (FL-MAC-M) or with different proton and neutron pairing gap parameters (FL-MAC-NP), in comparison with experiment. See text for details.

Estimation of the staggering effect for b coefficients of triplets shows that

$$b_{\text{pair}}^{T=1} = \begin{cases} 0, & A = 4n + 2, \\ 2(r_p - r_n)\dfrac{2^{1/3}B_s}{3A^{4/3}}, & A = 4n, \end{cases} \quad (40)$$

which results in a staggering amplitude $\Delta b = b(A) - b(A - 2)$ of

$$\Delta b^{T=1} \approx 2(r_n - r_p)\frac{2^{1/3}B_s}{3A^{4/3}}, \quad (41)$$

if we assume that $A = 4n + 2$. This is a factor of $1/(3A)$ or $1/A$ smaller as compared to the staggering in b coefficients for doublets or quartets, respectively (the effect cancels in the leading order of the Taylor expansion). As we can observe from Fig. 5, second panel, the staggering is indeed hardly visible on the scale of the figure, while the general trend is in robust agreement with experiment. The value of Δb obtained from FL-MAC-M is not shown in the plots for $T = 1$ (and $T = 2$), because it coincides with the present theoretical curve FL-MAC-NP in the scale of the figure.

Similarly, going further, we get that the staggering effect for b coefficients of quintets ($T = 2$) is negligible, as given by the analytical expression

$$\Delta b^{T=2} \approx -2(r_n - r_p)\frac{2^{1/3}B_s}{3A^{4/3}}, \quad (42)$$

assuming that $A = 4n + 2$. These are of the similar magnitude, but out of phase compared to those for triplets. For $T = 5/2$ multiplets, the staggering is again stronger, and in phase with the $T = 1/2$ pattern, being five times smaller in amplitude, according to

$$\Delta b^{T=5/2} \approx 2(r_n - r_p)\frac{2^{1/3}B_s}{5A^{1/3}}. \quad (43)$$

The resulting trends can be seen in Fig. 5 (last two panels). These patterns are expected to hold for higher half-integer and integer T multiplets. Future experiments will verify these predictions.

We remark that although the macroscopic part of the FRLDM can grasp the overall trend and phases of this peculiar staggering behavior, it can predict only a smooth variation of the staggering amplitude with mass because of the ansatz given by Eq. (27). This is due to the fact that the pairing effect is accounted in an average way. At the same time, we observe variations of the staggering amplitude in Fig. 5 which are probably related to the shell effects and the underlying microscopic structure of the many-nucleon systems. For example, for doublets, we notice stronger variations in b value for $A = 41$ and $A = 65, 67$ and oscillations of very small amplitude in the $f_{7/2}$ nuclei between $A = 43$ and $A = 53$ (Fig. 5, first panel). Similarly, various irregularities can be noticed for other multiplets. The macroscopic part of the FRLDM alone cannot account for these fine structures. It is an accurately added shell correction or a fully microscopic model which has to deal with these effects.

C. IMME beyond the second order

The mass excess parametrization proposed by the FRLDM allows one to extend the IMME beyond the second order in T_z. This can be done by expanding in Taylor series the contribution of the Coulomb exchange term up to the fourth order in T_z. The extended IMME thus would be of the form

$$M(\eta, T, T_z) = a(\eta, T) + b(\eta, T)T_z + c(\eta, T)T_z^2$$
$$+ d(\eta, T)T_z^3 + e(\eta, T)T_z^4, \quad (44)$$

where d and e coefficients come out to have the following expressions:

$$d = \frac{4c_4}{2^{1/3}81A^2}, \quad e = -\frac{40c_4}{2^{1/3}243A^3}. \quad (45)$$

Indeed, these quantities appear to be very small, the d coefficients are positive, while the e coefficients are always negative. The numerical values are larger for lower masses. For example, for $A = 17$, $d \approx 77$ eV and $e \approx -15$ eV, while for $A = 8$ these values would be about 350 eV and -150 eV, respectively. These values are considerably smaller than those few nonzero cases determined experimentally (which are all of the order of keV, e.g., Refs. [10,11]).
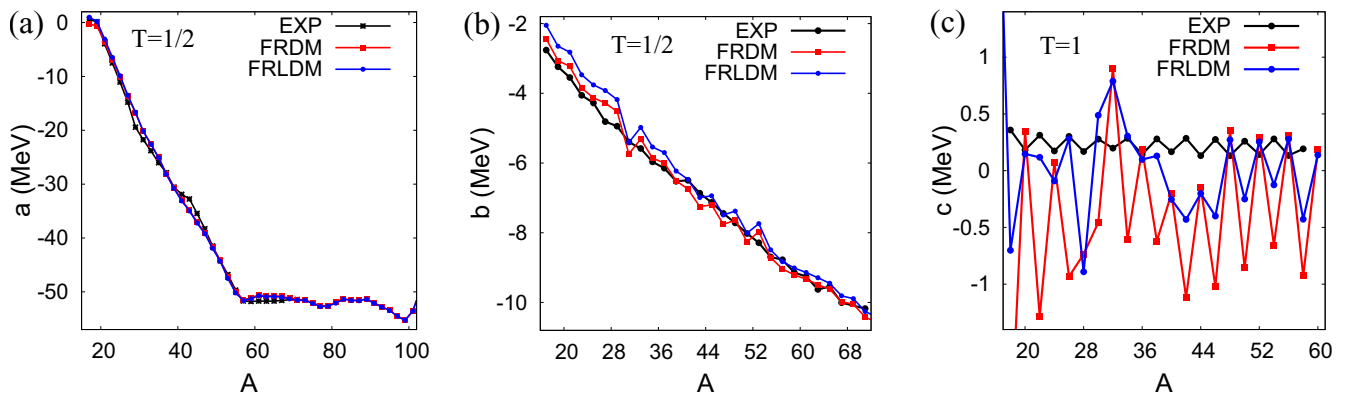

FIG. 6. Theoretical IMME a and b coefficients [panels (a) and (b), respectively] and c coefficients for triplets (c) obtained from the full FRDM and FRLDM in comparison with the experimental data. To deduce theoretical c coefficients we used theoretical masses from the FRDM/FRLDM and experimental excitation energies in $T_z = 0$ nuclei.
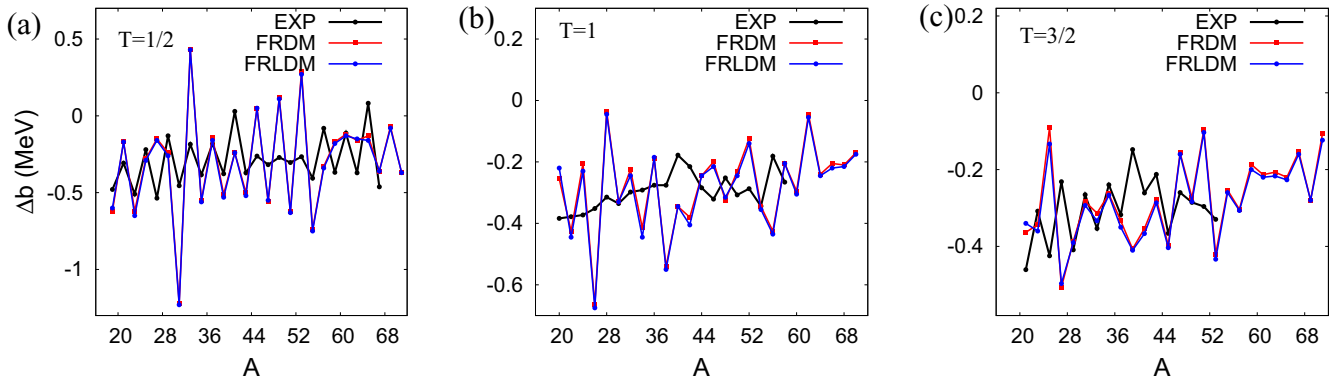
FIG. 7. Differences of IMME b coefficients, $\Delta b = b(A) - b(A - 2)$, for doublets (a), triplets (b), and quartets (c) as obtained from the FRDM and FRDLM in comparison with the experimental data.

There might be a specific contribution from the pairing term as well as from the proton form-factor, but these are expected to be of even smaller magnitude.

V. IMME COEFFICIENTS FROM THE FRLDM AND FRDM

In this section, we deduce the IMME a, b, and c coefficients using the mass predictions from the full FRDM and FRLDM for multiplets with $A > 16$ up to 101 for a coefficients, up to $A = 71$ for b coefficients, and up to $A = 60$ for c coefficients. The results obtained from the values of the mass compilation [33] are shown in Fig. 6, while the rms errors are summarized in Table I for both mass compilations, the one from 1995 [32] and the other from 2016 [33]. The overall rms errors are generally smaller for the latest set, with a few exceptions.

First, it is very well seen that both models, the FRDM and FRLDM, perfectly describe the a coefficients for doublets, reproducing the end of the strong downsloping trend up to $A \approx 57$. The predicted a coefficients for heavier nuclei along the $N = Z$ line are expected to stay roughly flat up to about $A \approx 90$ and to decrease in their absolute value towards $A = 100$. No data exist yet to compare with.

For b coefficients, the agreement between the two models (FRDM and FRLDM) and the data is less convincing compared to what we could obtain from the macroscopic part of the FRLDM only [cf. with Fig. 4(a)]. The corresponding rms errors, shown in Table I, support this conclusion. The staggering effect is plotted in Fig. 7 for doublets, triplets, and quartets and is seen to be too much exaggerated compared to the data and not always in phase with experiment. A similar conclusion is valid for c coefficients, which are shown in Fig. 6(c): the precision of the FRLDM/FRDM is not sufficient to describe the data in detail. The corresponding rms errors can be found in Table I. This conclusion is not surprising: the overall rms error of the models is 550 keV over almost the full mass chart (almost 2150 masses). Since b and c coefficients are linear combinations of two or three masses, the overall error may reach even higher values. This prevents the detailed description. We also believe that considering the experimental constraints on the b and c coefficients may help to improve on the modelization.

VI. MASSES OF PROTON-RICH NUCLEI UP TO $A = 100$

One of the major impacts of nuclear masses for heavy proton-rich nuclei is related to their importance for astrophysics, in particular, for type-I x-ray burst models [28]. Special attention from experiment and theory has been focused on the so-called waiting points of the rp process, e.g., ^{64}Ge, ^{68}Se, and ^{72}Kr [40]. The proton capture on these nuclei results in a proton-unbound or weakly bound nucleus and thus the β^+ decay may take over and divert the rp process path.

As nuclear mass increases along the $N = Z$ line, nuclei become more and more short lived due to increasing Coulomb effects and, as a result, it becomes harder and harder to discover them and determine their disintegration modes. Lots of experimental efforts have been devoted to explore the properties of very proton-rich nuclei and to trace the position of the proton drip line (e.g., Refs. [41–50]). Still, beyond Zr nuclei, astrophysical simulations rely only on atomic mass extrapolations [51] or on various theoretical predictions [9,26,52–57].

Since our best b coefficients obtained from the modified macroscopic part of the FRLDM with different proton and neutron pairing gaps (FL-MAC-NP) results in a relatively small rms error of known b coefficients of about 80 keV, we decided to use this model to calculate the masses of the proton-rich nuclei and thus to map the proton drip line. To reach this goal, we exploit the method of Coulomb displacement energies. Using the notations from Sec. II, $M(\eta, T, T_z) \equiv M_{T_z}$ for a given isotopic multiplet (η, T), we can express the mass excess of a proton-rich nucleus (with $T_z = -T$) on the basis of an experimental mass excess of its neutron-rich mirror (with $T_z = T$) and a theoretical b coefficient [26,52,54,58] as follows:

$$M_{-T} = M_T - 2\,b\,T. \qquad (46)$$

Theoretical b coefficients have been calculated using the proton-neutron version of the modified macroscopic part of the FRLDM (FL-MAC-NP). The experimental masses of neutron-rich nuclei and $N = Z$ nuclei have been taken from Ref. [51]. Thus, the mass excesses of nuclei with $Z > N$ have been obtained via Eq. (46). The resulting one- and two-proton separation energies (S_p and S_{2p}) for proton-rich nuclei with $25 \leqslant Z \leqslant 52$ and $-4 \leqslant T_z \leqslant -1/2$ are summarized in the
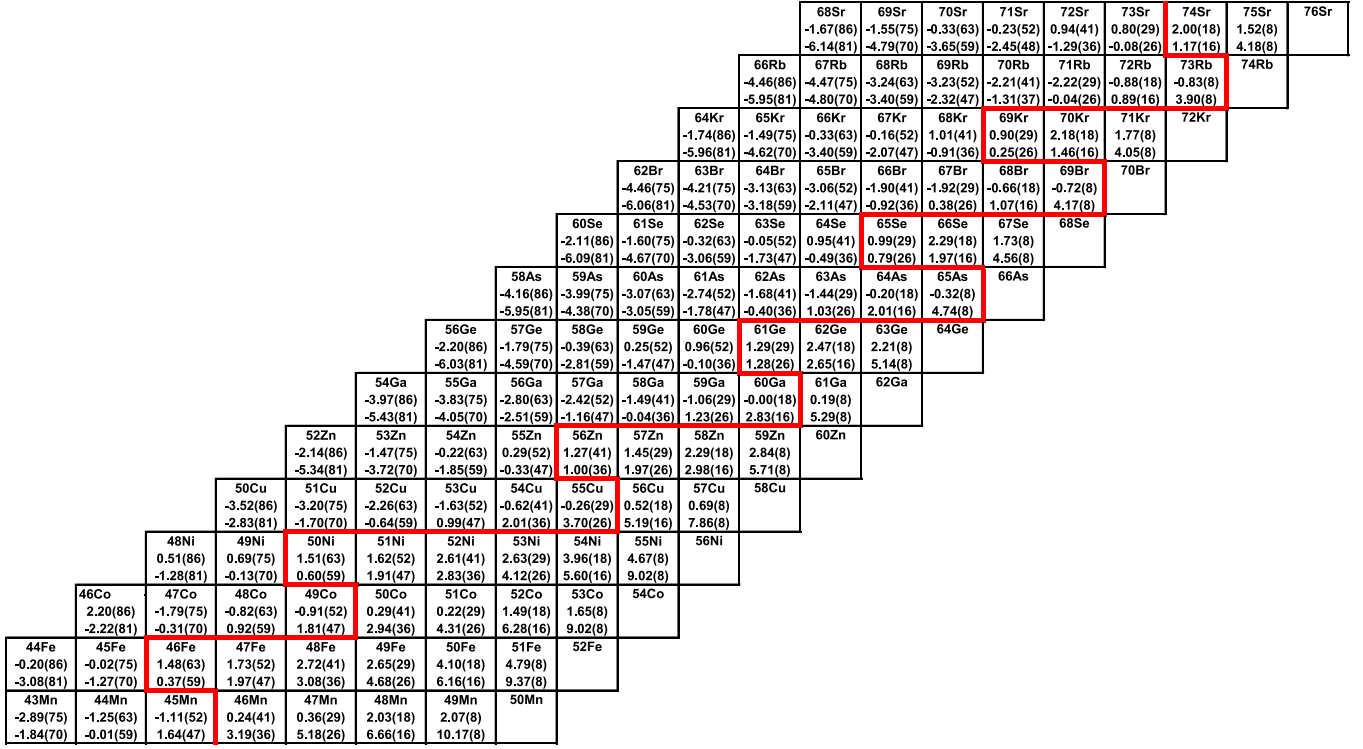
FIG. 8. A fragment of the nuclear chart for $Z > N$ nuclei with $25 \leqslant Z \leqslant 38$. Theoretical values of S_p and S_{2p} are indicated in each box below a nucleus symbol. The uncertainties are indicated in parentheses. The thick red line shows a tentative position of the proton drip line based on the average values of S_p and S_{2p}. See text for details.

Values in each box are given as: nuclide, S_p (upper), S_{2p} (lower). Boxes with only a symbol have no theoretical values.

Sr: 68Sr -1.67(86) / -6.14(81); 69Sr -1.55(75) / -4.79(70); 70Sr -0.33(63) / -3.65(59); 71Sr -0.23(52) / -2.45(48); 72Sr 0.94(41) / -1.29(36); 73Sr 0.80(29) / -0.08(26); 74Sr 2.00(18) / 1.17(16); 75Sr 1.52(8) / 4.18(8); 76Sr —

Rb: 66Rb -4.46(86) / -5.95(81); 67Rb -4.47(75) / -4.80(70); 68Rb -3.24(63) / -3.40(59); 69Rb -3.23(52) / -2.32(47); 70Rb -2.21(41) / -1.31(37); 71Rb -2.22(29) / -0.04(26); 72Rb -0.88(18) / 0.89(16); 73Rb -0.83(8) / 3.90(8); 74Rb —

Kr: 64Kr -1.74(86) / -5.96(81); 65Kr -1.49(75) / -4.62(70); 66Kr -0.33(63) / -3.40(59); 67Kr -0.16(52) / -2.07(47); 68Kr 1.01(41) / -0.91(36); 69Kr 0.90(29) / 0.25(26); 70Kr 2.18(18) / 1.46(16); 71Kr 1.77(8) / 4.05(8); 72Kr —

Br: 62Br -4.46(75) / -6.06(81); 63Br -4.21(70) / -4.53(70); 64Br -3.13(63) / -3.18(59); 65Br -3.06(52) / -2.11(47); 66Br -1.90(41) / -0.92(36); 67Br -0.66(18) / 0.38(26); 68Br -0.66(18) / 1.07(16); 69Br -0.72(8) / 4.17(8); 70Br —

Se: 60Se -2.11(86) / -6.09(81); 61Se -1.60(75) / -4.67(70); 62Se -0.32(63) / -3.06(59); 63Se -0.05(52) / -1.73(47); 64Se 0.95(41) / -0.49(36); 65Se 0.99(29) / 0.79(26); 66Se 2.29(18) / 1.97(16); 67Se 1.73(8) / 4.56(8); 68Se —

As: 58As -4.16(86) / -5.95(81); 59As -3.99(75) / -4.38(70); 60As -3.07(63) / -3.05(59); 61As -2.74(52) / -1.78(47); 62As -1.68(41) / -0.40(36); 63As -1.44(29) / 1.03(26); 64As -0.20(18) / 2.01(16); 65As -0.32(8) / 4.74(8); 66As —

Ge: 56Ge -2.20(86) / -6.03(81); 57Ge -1.79(75) / -4.59(70); 58Ge -0.39(63) / -2.81(59); 59Ge 0.25(52) / -1.47(47); 60Ge 0.96(52) / -0.10(36); 61Ge 1.29(29) / 1.28(26); 62Ge 2.47(18) / 2.65(16); 63Ge 2.21(8) / 5.14(8); 64Ge —

Ga: 54Ga -3.97(86) / -5.43(81); 55Ga -3.83(75) / -4.05(70); 56Ga -2.80(63) / -2.51(59); 57Ga -2.42(52) / -1.16(47); 58Ga -1.49(41) / -0.04(36); 59Ga -1.06(29) / 1.23(26); 60Ga -0.00(18) / 2.83(16); 61Ga 0.19(8) / 5.29(8); 62Ga —

Zn: 52Zn -2.14(86) / -5.34(81); 53Zn -1.47(75) / -3.72(70); 54Zn -0.22(63) / -1.85(59); 55Zn 0.29(52) / -0.33(47); 56Zn 1.27(41) / 1.00(36); 57Zn 1.45(29) / 1.97(26); 58Zn 2.29(18) / 2.98(16); 59Zn 2.84(8) / 5.71(8); 60Zn —

Cu: 50Cu -3.52(86) / -2.83(81); 51Cu -3.20(75) / -1.70(70); 52Cu -2.26(63) / -0.64(59); 53Cu -1.63(52) / 0.99(47); 54Cu -0.62(41) / 2.01(36); 55Cu -0.26(29) / 3.70(26); 56Cu 0.52(18) / 5.19(16); 57Cu 0.69(8) / 7.86(8); 58Cu —

Ni: 48Ni 0.51(86) / -1.28(81); 49Ni 0.69(75) / -0.13(70); 50Ni 1.51(63) / 0.60(59); 51Ni 1.62(52) / 1.91(47); 52Ni 2.61(41) / 2.83(36); 53Ni 2.63(29) / 4.12(26); 54Ni 3.96(18) / 5.60(16); 55Ni 4.67(8) / 9.02(8); 56Ni —

Co: 46Co 2.20(86) / -2.22(81); 47Co -1.79(75) / -0.31(70); 48Co -0.82(63) / 0.92(59); 49Co -0.91(52) / 1.81(47); 50Co 0.29(41) / 2.94(36); 51Co 0.22(29) / 4.31(26); 52Co 1.49(18) / 6.28(16); 53Co 1.65(8) / 9.02(8); 54Co —

Fe: 44Fe -0.20(86) / -3.08(81); 45Fe -0.02(75) / -1.27(70); 46Fe 1.48(63) / 0.37(59); 47Fe 1.73(52) / 1.97(47); 48Fe 2.72(41) / 3.08(36); 49Fe 2.65(29) / 4.68(26); 50Fe 4.10(18) / 6.16(16); 51Fe 4.79(8) / 9.37(8); 52Fe —

Mn: 43Mn -2.89(75) / -1.84(70); 44Mn -1.25(63) / -0.01(59); 45Mn -1.11(52) / 1.64(47); 46Mn 0.24(41) / 3.19(36); 47Mn 0.36(29) / 5.18(26); 48Mn 2.03(18) / 6.66(16); 49Mn 2.07(8) / 10.17(8); 50Mn —

form of two nuclear chart fragments shown in Figs. 8 and 9. The position of the one-proton or two-proton drip line is sketched by the thick read line, based on the central values of S_p for odd-Z isotopes or S_{2p} for even-Z isotopes, respectively.

The uncertainties on the obtained values of mass excesses of nuclei with $Z > N$ are estimated as

$$\Delta\left(M^{\text{th}}_{-T}\right) = \sqrt{\left[\Delta\left(M^{\text{exp}}_T\right)\right]^2 + 4\,T^2\left[\Delta(b_{\text{th}})\right]^2}, \qquad (47)$$

where $\Delta(b_{\text{th}}) \approx 81$ keV, estimated from the average rms error of theoretical b coefficients, while $\Delta(M^{\text{exp}}_T)$ refers to the uncertainty on the experimental mass excess of neutron-rich mirrors. It follows that, for the majority of cases, the uncertainty on the mass of a proton-rich nucleus, and therefore on the one- and two-proton separation energies, is mainly governed by the magnitude of the $2T\,\Delta(b_{\text{th}})$ term and, thus, is particularly large for high-T isobaric multiplets. Nevertheless, with increasing N and Z, the proton drip line approaches the $N = Z$ line and our results bring more accurate predictions for the stability of the nuclides of interest.

In general, we conclude that in spite of large uncertainties, our model provides a relatively robust picture of this exotic region of the nuclear chart and the position of the proton (and two-proton) drip line agrees for a majority of cases with the predictions of Ref. [9,26,54], taking into account the assigned theoretical uncertainties. Although we traced the drip line on the basis of the average values of S_p and S_{2p}, often the uncertainty may allow shifting it one nucleus left or right.

The nuclear chart fragments in Figs. 8 and 9 contain in total 220 theoretical S_p and S_{2p} values. From these numbers, only 103 sets of S_p and S_{2p} can be calculated based on the masses present in the AME2016 database [51] (24 experimentally measured masses and 79 extrapolated values). Overall, our calculated theoretical one- and two-proton separation energies are in fair agreement with these data. To address the quality of the results, we have calculated the rms error according to Eq. (34) with x being either S_p or S_{2p}. We find that $\text{rmse}(S_p) = 320$ keV and $\text{rmse}(S_{2p}) = 353$ keV for a total number of $n = 103$ data points.

We note, however, that extrapolated masses in AME2016 [51] may contain big associated uncertainties and therefore the application of Eq. (34) may not be an optimal choice. If we exclude all extrapolated masses in Ref. [51] and estimate the rms error for the 24 experimentally measured cases, we get $\text{rmse}(S_p) = 148$ keV and $\text{rmse}(S_{2p}) = 154$ keV. In addition, we have calculated the χ^2 per number of degrees of freedom (χ^2/ν) with $\nu = n - 1$,

$$\chi^2/\nu = \frac{1}{n-1}\sum_{i=1}^{n}\frac{[S_{\text{th}}(i) - S_{\text{exp}}(i)]^2}{\sigma_{\text{th}}^2(i) + \sigma_{\text{exp}}^2(i)}, \qquad (48)$$

and get that, for $n = 24$ experimentally measured cases, $\chi^2/\nu = 0.88$ for S_p, while $\chi^2/\nu = 0.94$ for S_{2p}. These close to the unity estimates show that the theoretical outcome is reasonable.

Now, let us briefly discuss the results. In the lower part of the nuclear chart (Fig. 8), the position of the drip line and

Te: 96Te −4.25(86) / −9.93(81) · 97Te −3.96(75) / −9.16(70) · 98Te −3.35(63) / −8.28(59) · 99Te −3.22(52) / −7.53(49) · 100Te −2.60(41) / −6.85(37) · 101Te −2.56(40) / −6.17(44)

Sb: 94Sb −6.01(86) / −7.77(81) · 95Sb −5.68(75) / −6.76(70) · 96Sb −5.21(63) / −6.22(59) · 97Sb −4.93(52) / −5.15(47) · 98Sb −4.31(42) / −4.44(38) · 99Sb −4.26(30) / −3.51(39) · 100Sb −3.61(39) / −2.57(39)

Sn: 92Sn −1.85(86) / −5.94(81) · 93Sn −1.76(75) / −4.96(70) · 94Sn −1.08(63) / −4.29(59) · 95Sn −1.01(52) / −3.24(47) · 96Sn −0.22(41) / −2.48(36) · 97Sn −0.12(33) / −1.33(41) · 98Sn 0.75(35) / −0.50(44) · 99Sn 1.04(43) / 1.78(43)

In: 90In −4.10(86) / −5.67(81) · 91In −4.10(75) / −4.96(70) · 92In −3.19(63) / −3.94(59) · 93In −3.21(52) / −3.16(47) · 94In −2.23(41) / −2.23(36) · 95In −2.26(29) / −1.17(40) · 96In −1.21(36) / −0.03(44) · 97In −1.24(51) / 2.02(43) · 98In

Cd: 88Cd −1.74(86) / −6.06(81) · 89Cd −1.57(75) / −4.97(70) · 90Cd −0.86(63) / −4.23(59) · 91Cd −0.75(52) / −3.12(47) · 92Cd 0.05(41) / −2.29(36) · 93Cd 0.00(29) / −1.26(39) · 94Cd 1.09(35) / −0.18(34) · 95Cd 1.18(51) / 1.88(43) · 96Cd

Ag: 86Ag −4.27(86) / −5.90(81) · 87Ag −4.32(75) / −5.11(70) · 88Ag −3.40(64) / −4.24(59) · 89Ag −3.37(52) / −3.15(47) · 90Ag −2.37(41) / −2.23(39) · 91Ag −2.34(29) / −1.29(39) · 92Ag −1.27(35) / 0.03(34) · 93Ag −1.27(43) / 2.03(43) · 94Ag

Pd: 84Pd −1.74(86) / −6.22(81) · 85Pd −1.64(75) / −5.21(70) · 86Pd −0.79(63) / −4.30(59) · 87Pd −0.84(52) / −3.25(47) · 88Pd 0.22(41) / −2.26(36) · 89Pd 0.14(33) / −1.13(26) · 90Pd 1.05(35) / −0.29(34) · 91Pd 1.29(43) / 2.02(43) · 92Pd

Rh: 82Rh −4.53(86) / −6.40(81) · 83Rh −4.48(75) / −5.14(70) · 84Rh −3.57(63) / −4.58(59) · 85Rh −3.51(52) / −3.14(47) · 86Rh −2.41(41) / −2.48(36) · 87Rh −2.48(29) / −1.02(26) · 88Rh −1.27(24) / −0.28(37) · 89Rh −1.34(43) / 2.60(31) · 90Rh

Ru: 80Ru −1.70(86) / −6.26(81) · 81Ru −1.87(75) / −5.31(70) · 82Ru −0.66(63) / −4.26(59) · 83Ru −1.00(52) / −3.47(47) · 84Ru 0.37(41) / −2.16(36) · 85Ru −0.08(29) / −1.23(30) · 86Ru 1.46(18) / −0.01(34) · 87Ru 0.98(31) / 2.33(8) · 88Ru

Tc: 78Tc −4.61(86) / −6.37(81) · 79Tc −4.56(75) / −5.25(70) · 80Tc −3.45(63) / −4.28(59) · 81Tc −3.60(52) / −3.46(47) · 82Tc −2.46(41) / −2.59(36) · 83Tc −2.53(29) / −1.06(27) · 84Tc −1.15(24) / −0.38(34) · 85Tc −1.47(31) / 2.43(17) · 86Tc

Mo: 76Mo −1.62(86) / −6.04(81) · 77Mo −1.76(75) / −4.95(70) · 78Mo −0.69(63) / −3.90(59) · 79Mo −0.83(52) / −3.09(47) · 80Mo 0.14(41) / −1.92(36) · 81Mo −0.13(29) / −1.16(27) · 82Mo 1.45(21) / 0.22(34) · 83Mo 0.77(35) / 2.69(20) · 84Mo

Nb: 74Nb −4.47(86) / −6.00(81) · 75Nb −4.42(75) / −4.68(70) · 76Nb −3.19(63) / −3.61(59) · 77Nb −3.21(52) / −2.76(47) · 78Nb −2.26(41) / −2.15(36) · 79Nb −2.06(29) / −0.93(26) · 80Nb −1.03(20) / 0.37(34) · 81Nb −1.26(33) / 2.57(15) · 82Nb

Zr: 72Zr −1.58(86) / −6.15(81) · 73Zr −1.53(75) / −5.10(70) · 74Zr −0.26(63) / −3.81(59) · 75Zr −0.43(52) / −2.69(47) · 76Zr 0.45(41) / −1.47(36) · 77Zr 0.11(29) / −0.53(26) · 78Zr 1.13(18) / 0.78(17) · 79Zr 1.41(32) / 3.06(11) · 80Zr

Y: 70Y 4.34(86) / −5.89(81) · 71Y −4.57(75) / −4.90(70) · 72Y −3.58(63) / −3.81(59) · 73Y −3.55(52) / −2.61(47) · 74Y −2.27(41) / −1.46(36) · 75Y −1.91(29) / 0.09(26) · 76Y −0.64(18) / 0.88(16) · 77Y −0.35(9) / 3.98(8) · 78Y

FIG. 9. A fragment of the nuclear chart for $Z > N$ nuclei with $39 \leqslant Z \leqslant 52$. Theoretical values of S_p and S_{2p} are indicated in each box below the nucleus symbol. The uncertainties are indicated in parentheses. The thick red line shows a tentative position of the proton drip line based on the average values of S_p and S_{2p}. See text for details.

the properties of near lying nuclei are largely known experimentally [59,60]. According to our calculation, the odd-Z nuclei ^{45}Mn, ^{49}Co, ^{55}Cu, ^{59}Ga are proton unbound. ^{50}Co is obtained to be weakly bound, although our large uncertainty does not exclude the possibility that it is proton unbound. The one-proton separation energy in ^{60}Ga is obtained to be zero with an uncertainty of 180 keV, however. At the same time, ^{54}Cu is expected in our model to be proton unbound with $|S_p| < 1$ MeV.

For even-Z ^{49}Ni, ^{55}Zn, ^{60}Ge, ^{64}Se, ^{68}Kr, ^{73}Sr we find $S_p > 0$, while $S_{2p} < 0$; however, these $|S_{2p}|$ values stay rather small. Indeed, all of these nuclei have been observed [43,47,50,61]. Some of them have tentatively been proposed as potential candidates for two-proton radioactivity according to experimental indications, while β decay might still be the preferred decay mode for a few of them (e.g., for ^{49}Ni [61], ^{68}Kr [62], and ^{73}Sr [50]). Their neighbors with one neutron less, ^{48}Ni, ^{54}Zn, ^{59}Ge, ^{63}Se, ^{67}Kr, ^{72}Sr, as well as ^{45}Fe, are calculated to have a more pronounced and negative S_{2p} and thus may be considered as possible candidates for $2p$ emission (confirmed for ^{45}Fe [63,64], ^{48}Ni [65,66], ^{54}Zn [42], and ^{67}Kr [67]). At the same time, ^{59}Ge and ^{63}Se have been observed to disintegrate via β decay [67], which may not be surprising, since the predicted $|S_{2p}|$ value is smaller than the one found for ^{67}Kr (see also a recent study from ^{78}Kr fragmentation reported in Ref. [47]).

For heavier odd-Z nuclei, we report on the possibility of negative S_p values for ^{64,65}As, ^{68,69}Br, ^{71,72,73}Rb, which is in accord with experimental studies of those nuclei [44,46,49,50,68]. The less negative S_p values for ^{64,65}As are in agreement with the fact that those nuclei have been observed experimentally [41,68], while ^{69}Br and ^{73}Rb, having more negative S_p values, were not observed [44,46,49] and, therefore, may be proton-unbound with a very short half-life. Among these nuclei are the rp-process waiting-point neighbors, ^{65}As, ^{69}Br and ^{73}Rb, which have thus important implication for astrophysics simulations.

We notice another interesting feature for a few series of odd-Z isotopes, namely, we indeed observe the existence of the so-called "sandbanks" [49]: S_p for an even A nucleus can be similar or even less negative than for an odd-mass $(A + 1)$ nucleus. It is well illustrated by numerous examples from our chart, e.g., ^{68}Br–^{69}Br, ^{66}Br–^{67}Br, ^{72}Rb–^{73}Rb, ^{70}Rb–^{71}Rb, and heavier ^{80}Nb–^{81}Nb, etc.

For ^{76,77}Y, our S_p values stay small, but negative, within relatively small error bars (see Fig. 9), which is not completely excluded by the results on β-decay half-lives of these isotopes deduced from the experimental studies [45,50]. At the same time, we remark on a very good agreement with the experimental indications for ^{81}Nb, ^{85}Tc, ^{89}Rh, ^{93}Ag, and ^{97}In to be proton unbound (see Refs. [45,48]). In particular, we find that our theoretical one-proton separation energies for ^{89}Rh, ^{93}Ag,

and ^{97}In are close to experimentally determined values [48]. Similarly, we confirm a general tendency of a decrease of $|S_p|$ and, therefore, of an increase of stability, when approaching $Z = 50$ (see a slight change in the average value of S_p when going from ^{85}Tc to ^{89}Rh, ^{93}Ag and further to ^{97}In). These are the nuclei which result from a proton-capture on even-even $N = Z$ nuclei (possible waiting points).

For even-Z Sr and Zr, according to our calculation, ^{73}Sr and ^{77}Zr are slightly unbound, with the S_{2p} value being close to zero. At the same time, we find ^{82}Mo slightly bound with respect to two-proton emission, with a large uncertainty, however.

For the heavy even-even nuclei ^{86}Ru, ^{90}Pd, ^{94}Cd, ^{98}Sn, we get $S_p > 0$ and $S_{2p} < 0$, with S_{2p} being very small. Due to this reason, we would be cautious to provide any definite answer about the exact position of the two-proton drip line here. Their neighbors with one neutron less, ^{85}Ru, ^{89}Pd, ^{93}Cd, ^{97}Sn, are predicted to have $-1.5 \lesssim S_{2p} \lesssim -1$ (MeV), and thus are expected be two-proton unbound. However, one might need to go to still more exotic isotopes, ^{84}Ru, ^{88}Pd, ^{92}Cd, or ^{96}Sn, in a search for plausible candidates for $2p$ emission.

We remark that the masses of heaviest $T_z = -1/2$ nuclei from ^{89}Rh to ^{99}Sn are based on the extrapolated masses of their $T_z = 1/2$ mirrors [51]. Beyond Sn isotopes, we cannot approach the $N = Z$ line with our calculation, since the mass excesses of neutron-rich mirrors become unknown.

Addition of the proper shell correction, capable of reproducing variations of b coefficients in a better way, would in principle reduce the uncertainty on the proton and two-proton separation energies, and it could also modify their central values.

VII. CONCLUSIONS AND SUMMARY

In the present work, we have applied the macro-microscopic approach of P. Möller and collaborators, the FRDM and FRLDM, to estimate the IMME a and b coefficients in nuclei in the vicinity of $N = Z$ until $A \approx 100$. We found that the macroscopic part of the FRLDM, representing a refined version of the well-known liquid-drop model, is rather well suited to describe the general trends of the coefficients. In particular, introduction of proton and neutron pairing energy parameters adjusted to experiment allowed us to reproduce the staggering effect of b coefficients in very good agreement with the data.

The full FRDM and FRLDM approaches prove to be advantageous in providing the general trend of the a coefficients towards heavier nuclei along the $N = Z$ line, which would be interesting to confirm experimentally. However, the description of b and c coefficients is not satisfactory. This may hint at a possible opportunity to improve the parametrizations with a specific consideration of the isovector and isotensor parts of the total energy.

The "best" set of b coefficients obtained from the modified macroscopic part of FRLDM is used to calculate the masses of proton-rich nuclei based on experimental masses of their neutron-rich mirrors and theoretical b coefficients. The results obtained on one- and two-proton separation energies of nuclei in the vicinity of the proton drip line are in robust agreement with the available experimental data. The predictions made for heavier nuclei near ^{100}Sn can serve to guide future experiments.

We hope that our study can motivate further exploration and developments of the FRDM and FRLDM, aiming at a better description of the isospin degree of freedom, which could in future provide the community with more accurate predictions of masses of proton-rich nuclei. The properties of those nuclei up to $A \approx 100$ are very important for simulations of the astrophysical rp process.

[1] W. Heisenberg, Z. Phys. **77**, 1 (1932).

[2] E. P. Wigner, in *Proceedings of the Robert A. Welch Foundation Conference on Chemical Research*, edited by W. O. Milligan (Welch Foundation, Houston, 1957), Vol. 1, p. 86.

[3] J. Jänecke and P. Masson, At. Data Nucl. Data Tables **39**, 265 (1988).

[4] J. Jänecke, Phys. Rev. **147**, 735 (1966).

[5] K. T. Hecht, in *Isobaric Spin in Nuclear Physics*, edited by J. D. Fox and D. Robson (Academic, New York, 1966), p. 823.

[6] K. T. Hecht, Nucl. Phys. A **102**, 11 (1967).

[7] J. Jänecke, in *Systematics of Coulomb Energies and Excitation Energies of Isobaric Analogue States, Isospin in Nuclear Physics*, edited by D. H. Wilkinson (North-Holland, Amsterdam, 1969), p. 297.

[8] Y. H. Lam, N. A. Smirnova, and E. Caurier, Phys. Rev. C **87**, 054304 (2013).

[9] K. Kaneko, Y. Sun, T. Mizusaki, and S. Tazaki, Phys. Rev. Lett. **110**, 172505 (2013).

[10] Y. H. Lam *et al.*, At. Data Nucl. Data Tables **99**, 680 (2013).

[11] M. MacCormick and G. Audi, Nucl. Phys. A **925**, 61 (2014).

[12] X. L. Tu *et al.*, J. Phys. G: Nucl. Part. Phys. **41**, 025104 (2014).

[13] W. E. Ormand, B. A. Brown, and M. Hjorth-Jensen, Phys. Rev. C **96**, 024323 (2017).

[14] P. Baczyk *et al.*, Phys. Lett. B **778**, 178 (2018).

[15] G. J. Fu, Y. Y. Cheng, Y. H. Zhang, P. Zhang, P. Shuai, Y. M. Zhao, and M. Wang, Phys. Rev. C **97**, 024339 (2018).

[16] M. Brodeur *et al.*, Phys. Rev. C **96**, 034316 (2017).

[17] E. Henley and C. Lacy, Phys. Rep. **184**, 1228 (1969).

[18] J. Jänecke, Nucl. Phys. A **128**, 632 (1969).

[19] G. F. Bertsch and S. Kahana, Phys. Lett. B **33**, 193 (1970).

[20] W. Benenson and E. Kashy, Rev. Mod. Phys. **51**, 527 (1979).

[21] A. Signoracci and B. A. Brown, Phys. Rev. C **84**, 031301(R) (2011).

[22] J. M. Dong, Y. H. Zhang, W. Zuo, J. Z. Gu, L. J. Wang, and Y. Sun, Phys. Rev. C **97**, 021301(R) (2018).

[23] J. M. Dong, J. Z. Gu, Y. H. Zhang, W. Zuo, L. J. Wang, Y. A. Litvinov, and Y. Sun, Phys. Rev. C **99**, 014319 (2019).

[24] W. E. Ormand and B. A. Brown, Nucl. Phys. A **491**, 1 (1989).

[25] W. E. Ormand, Phys. Rev. C **53**, 214 (1996).

[26] W. E. Ormand, Phys. Rev. C **55**, 2407 (1997).

[27] P. Baczyk, W. Satula, J. Dobaczewski, and M. Konieczka, J. Phys. G **46**, 03LT01 (2019).

[28] H. Schatz *et al.*, Phys. Rep. **294**, 167 (1998).

[29] R. K. Wallace and S. E. Woosley, Astrophys. J. Suppl. **45**, 389 (1981).

[30] R. Cyburt *et al.*, Astrophys. J. **830**, 55 (2016).

[31] H. Grawe, G. Martínez-Pinedo, and K. Langanke, Rep. Prog. Phys. **70**, 1525 (2007).

[32] P. Möller and J. R. Nix, At. Data Nucl. Data Tables **59**, 185 (1995).

[33] P. Möller, A. J. Sierk, T. Ichikawa, and H. Sagawa, At. Data Nucl. Data Tables **109-110**, 1 (2016).

[34] M. A. Bentley and S. M. Lenzi, Prog. Part. Nucl. Phys. **59**, 497 (2007).

[35] H. A. Bethe and R. F. Bacher, Rev. Mod. Phys. **8**, 82 (1936).

[36] A. Bohr and B. Mottelson, *The Nuclear Structure*, 2nd corrected and enlarged ed. (Springer-Verlag, Heidelberg, 1977).

[37] J. A. Nolen and J. P. Schiffer, Annu. Rev. Nucl. Sci. **19**, 471 (1969).

[38] J. Jänecke, Phys. Rev. C **11**, 625 (1975).

[39] P. Möller and J. R. Nix, Nucl. Phys. A **536**, 20 (1992).

[40] H. Schatz, A. Aprahamian, V. Barnard, L. Bildsten, A. Cumming, M. Ouellette, T. Rauscher, F. K. Thielemann, and M. Wiescher, Phys. Rev. Lett. **86**, 3471 (2001).

[41] B. Blank *et al.*, Phys. Rev. Lett. **74**, 4611 (1995).

[42] B. Blank *et al.*, Phys. Rev. Lett. **94**, 232501 (2005).

[43] A. Stolz *et al.*, Phys. Lett. B **627**, 32 (2005).

[44] A. M. Rogers *et al.*, Phys. Rev. Lett. **106**, 252503 (2011).

[45] T. Faestermann *et al.*, Eur. Phys. J. A **15**, 185 (2002).

[46] M. Del Santo *et al.*, Phys. Lett. B **738**, 453 (2014).

[47] B. Blank *et al.*, Phys. Rev. C **93**, 061301 (2016).

[48] I. Čeliković *et al.*, Phys. Rev. Lett. **116**, 162501 (2016).

[49] H. Suzuki *et al.*, Phys. Rev. Lett. **119**, 192503 (2017).

[50] L. Sinclair *et al.*, Phys. Rev. C **100**, 044311 (2019).

[51] M. Wang *et al.*, Chin. Phys. C **41**, 030003 (2017).

[52] B. A. Brown, Phys. Rev. C **43**, R1513 (1991).

[53] B. J. Cole, Phys. Rev. C **54**, 1240 (1996).

[54] B. A. Brown, R. R. C. Clement, H. Schatz, A. Volya, and W. A. Richter, Phys. Rev. C **65**, 045802 (2002).

[55] G. Lalazissis, D. Vretenar, and P. Ring, Nucl. Phys. A **679**, 481 (2001).

[56] E. Olsen, M. Pfutzner, N. Birge, M. Brown, W. Nazarewicz, and A. Perhac, Phys. Rev. Lett. **110**, 222501 (2013).

[57] B. A. Brown, B. Blank, and J. Giovinazzo, Phys. Rev. C **100**, 054332 (2019).

[58] A. Pape and M. S. Antony, At. Data Nucl. Data Tables **39**, 201 (1988).

[59] B. Blank and M. J. G. Borge, Prog. Part. Nucl. Phys. **60**, 403 (2008).

[60] M. Pfützner, M. Karny, L. V. Grigorenko, and K. Riisager, Rev. Mod. Phys. **84**, 567 (2012).

[61] J. Giovinazzo *et al.*, Eur. Phys. J. A **10**, 73 (2001).

[62] J. Giovinazzo *et al.*, Acta Phys. Pol. B **51**, 577 (2020).

[63] J. Giovinazzo *et al.*, Phys. Rev. Lett. **89**, 102501 (2002).

[64] M. Pfützner *et al.*, Eur. Phys. J. A **14**, 279 (2002).

[65] C. Dossat *et al.*, Phys. Rev. C **72**, 054315 (2005).

[66] M. Pomorski *et al.*, Phys. Rev. C **83**, 061303(R) (2011).

[67] T. Goigoux *et al.*, Phys. Rev. Lett. **117**, 162501 (2016).

[68] X. L. Tu *et al.*, Phys. Rev. Lett. **106**, 112501 (2011).